energy&fuels

Article

pubs.acs.org/EF

Macro- and Microscale Waterflooding Performances of Crudes which form w/o Emulsions upon Mixing with Brines

N. Rezaei[†] and A. Firoozabadi*[,†,‡]

[†]Reservoir Engineering Research Institute, 595 Lytton Avenue, Palo Alto, California 94301, United States

[‡]Yale University, New Haven, Connecticut 06520, United States

ABSTRACT: We study the micro- and macroscale waterflooding performances of unusual crudes which naturally form tight emulsions (stable after 15 months) upon mixing with water and different brines—including the reservoir brine. These crudes are obtained from a large oil field with stock tank oil viscosities in the range 20−100 cP. The waterflooding tests are conducted at constant injection rates in Berea cores and also in a glass-etched micromodel with and without initial water saturation. With the initial water saturation, the emulsions cause final oil recovery to be significantly lower while the breakthrough is surprisingly suppressed. Pressure data suggests that emulsions are formed in situ in the waterflooding tests both with and without the initial water saturation. The injection pressure data show significant fluctuations after about 3 pore volumes of injection. Both the pressure drop and pressure fluctuations are found to be higher at lower injection rates. Furthermore, the pressure drop is higher in tests with the initial water saturation, which may be related to the formation of water-in-oil (w/o) emulsions during the oil injection into water-saturated cores and subsequent aging. We also observe a pronounced initial pressure spike, which cannot be described by the bulk oil rheology as the oil exhibits only a mild shear thinning behavior. The coreflooding results are qualitatively explained from the viewpoint of deep-bed filtration. The pore-scale waterflooding results reveal the formation of both w/o microemulsions and macroemulsions. We observe the accumulation of w/o emulsions at the oil/water interface and in the dead-end pore spaces. Large emulsion droplets are observed to block a significant portion of a pore, which may be re-entrained and mobilized at higher rates. Overall, the formation of w/o emulsions results in significant production challenges because of high pressure drops, especially for the flow initialization.

1. INTRODUCTION

Emulsion flow in porous media has been found attractive in the oil industry after McAuliffe utilized the oil-in-water (o/w) emulsions for improved oil recovery by waterflooding.[1,2] The emulsion flow in porous media becomes important in the processes such as waterflooding, surfactant flooding, alkaline flooding, acidizing, and steam flooding. The emulsions can form in situ by adding surfactant or naturally. In the natural formation, the reaction between alkali and acidic functional parts of crude components may produce surfactants at the water/oil interface.[3] These surfactants can help to form and stabilize emulsions in situ by encapsulating the dispersed liquid phase through a dense interfacial film. Fine solid particles such as clay, sand, asphaltenes, corrosion products, mineral scales, and drilling muds can also adsorb at the interfacial area and stabilize the emulsion,[4] if they are wetted by both phases, and also if they are much smaller than the emulsion droplets.[5]

Emulsification in the form of o/w has been proven a successful oil recovery mechanism for conventional oils. This idea is recently revitalized for the recovery of heavy crudes by alkali/surfactant flooding.[6−11] The viscosity of o/w emulsion can be lower than that of the heavy oil and the formation of o/w emulsion may also decrease the mobility contrast between displacing and displaced phases. In several alkaline-surfactant flooding experiments (with heavy oils), w/o emulsion formation is observed, especially in brines with high salt concentrations and multiple cations such as Ca^{2+} and Mg^{2+}.[6,8,9,12−14] The viscosity of w/o emulsions can be significantly higher than the oil, resulting in a large pressure drop across injection and production wells. Therefore, the formation of w/o emulsions in alkali-surfactant flooding is undesirable, especially for viscous crudes.

The flow of emulsions in porous media is very complex. The process is often studied from two different perspectives: (1) continuum liquid flow[15] and (2) deep-bed filtration theory.[16−19] In the first view, the emulsion is considered a single-phase liquid continuum with higher viscosity (compared to its continuous phase), and the effect of injection rate on emulsion flow is considered by rheology of the emulsion phase. In the filtration theory, two mechanisms of straining and interception are used to describe the velocity-dependency of the emulsion flow.[18] Emulsion drop size distribution, pore structure, surface chemistry of the solid grains, interfacial tension, zeta potential, ionic strength, and hydrodynamics of the injecting fluid govern the emulsion flow in porous media.[17] Not only the droplets larger than the pore throat can block flow by constricting pore throat (straining) but also smaller droplets can block flow by attaching to surface of pore grains, or by being retained in the convex pore spaces between grains, and also in the pore pockets with stagnant or recirculation eddies (interception).[17] The strained droplets can later squeeze through pore constrictions at high injection rates, or can break up by snap off or viscous shear mechanisms. Re-entrainment to the main flow stream can occur at high rates for droplets captured by the interception process.[18] The droplet capturing and re-entrainment exhibit dynamic local pressure fluctuations.

Received: November 9, 2013
Revised: January 23, 2014
Published: January 27, 2014

Table 1. Brine Compositions Used in the Emulsion Analysis and Waterflooding Tests

	salt concentration (mg/L) in brine										
salt	IW	Q	C	K	1	2	3	4	5	6	7
NaCl	88 720	28 390			5500			5500	5500		5500
KCl	9534	3051		1000		800		800		800	800
$CaCl_2$	21 877	7000	3000				1300		1300	1300	1300
$MgCl_2$	10 969	3510									

Table 2. Physical Properties of Oils and Brines at Room Temperature (25 °C)

		physical property			
fluid	designation	μ (cP)	ρ (g/cm^3)	σ (mN/m)	pH
brine	Q	1.031 ± 0.002	1.008 ± 0.002	72.78 ± 0.38	6.78 ± 0.01
	C	0.996 ± 0.001	1.000 ± 0.003	62.55 ± 0.35	6.70 ± 0.01
oil	n-C_7	0.420 ± 0.001	0.684 ± 0.000	19.95 ± 0.048	n/a
	QO-2	19.272 ± 0.058	0.876 ± 0.002	28.50 ± 0.02	n/a
	QO-9	82.155 ± 0.161	0.919 ± 0.002	30.44 ± 0.02	n/a
	QO-13	25.618 ± 0.156	0.888 ± 0.001	27.23 ± 0.01	n/a

In this research, we aim to investigate the micro- and macroscale waterflooding performances of three different crudes that naturally form emulsions upon mixing with brine or water. The effect of injection rate, crude oil, and initial water saturation is studied. Our work is different from a surfactant, alkaline, or surfactant-alkaline flooding, which are extensively discussed in the literature.[14,20−24] We do not add chemicals (surfactant, acid, or base) to the brine; yet we find micro- and macroscale evidence that microemulsions form in situ upon waterflooding.

This paper is structured along the following lines. We first present the brines, crudes and other fluids, cores, and the micromodel used in our work. Then, we describe the experimental setup and the procedure for saturation establishment and waterflooding in the core and the micromodel. In the next section, results from emulsions, waterflooding in the cores, and waterflooding in the micromodel are presented and analyzed. At the end, we present our conclusions.

2. EXPERIMENTAL SECTION

2.1. Test Fluids. In total, we use 11 different brines for the waterflooding and emulsion analysis tests as summarized in Table 1. We use nine different brines for the emulsion analysis (brines 1−7 and brines Q and K, in Table 1) and four brines for the waterflooding tests (IW, Q, C, and K).

In the waterflooding experiments, CO_2 and N_2 gases, n-heptane (Macron Chemicals, 99.0%), purified water, four different brines (IW, Q, C, and K), and three different crudes (QO-2, QO-9, and QO-13) are used. The density, viscosity, surface tension of oils and brines, and the pH of brines used in the waterflooding tests are shown in Table 2. In this table, μ, ρ, and σ are the viscosity, density, and surface tension of the liquids, respectively. For the crudes, the physical properties are measured after oil pretreatment, so they show dead oil properties. The asphaltene content of the three crudes is generally low, around 1 wt %. Most likely, the heteroatoms in the asphaltenes cause emulsion formation with water and brine. The brine compositions are shown in Table 1. In the core cleaning, we use different solvents such as toluene (BDH, 99.5%), methanol (Cole-Parmer, 98.8%), isopropyl alcohol (IPA) (Cole-Parmer, 99.5%), methylene chloride (Fisher Scientific, 99.9%), and chromic acid (Ricca Chemical, 10% w/v).

The crude samples contained emulsions when received in the lab. We use a centrifuge to obtain emulsion-free crudes for the waterflooding experiments. The oil is first centrifuged at 8000 rpm (equivalent to ∼10 000g) for a period of 1 h. In the centrifuge, the oil, emulsion, water, and sand are separated, as shown in Figure 1. Crude QO-9 has substantial amounts of brine, w/o emulsion and sand along with the emulsion-free oil, while crude QO-2 has mostly emulsion-free oil with some w/o emulsions.

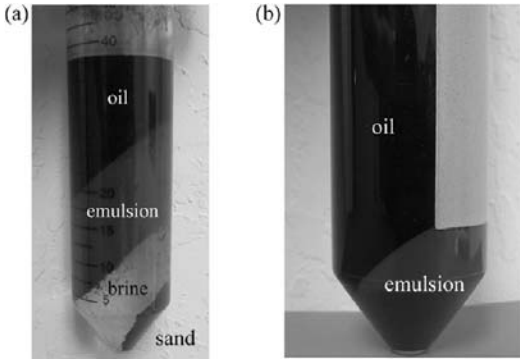

Figure 1. Snap shots of oil samples (a) QO-9 and (b) QO-2 from centrifugation at 8000 rpm for a period 1 h.

The oil is separated from the rest and is heated to 50 °C for 1 h under reflux conditions, removing volatile components to avoid the formation of a vapor phase in the waterflooding experiments.

As observed in Figure 1, a layer of excess water exists in the vial of crude QO-9 but not in crude QO-2. The former crude was supplied in a container with more than 75% (by volume) of reservoir brine Q, while the raw crude QO-2 did not have excess water.

2.2. Porous Media. We conduct the waterflooding experiments in cores (fired and unfired) and in glass micromodel (for visual tests). The characteristics of porous media are summarized in the following.

2.2.1. Berea Cores. Two different groups of Berea sandstone cores are obtained from Cleveland quarries with the porosities of 20.0 to 22.8% and the initial absolute permeability to brine (K_b^0) of 192 to 630 mD. Table 3 provides the core properties in which T_f is the firing

Table 3. Relevant Data of Fired and Unfired Berea Cores[a]

	dimensions (cm)					
core	L	D	PV (mL)	ϕ (% PV)	K_b^0(mD)	T_f (°C)
B2N	14.595	3.815	35.54	21.31	273.7	n/a
B3N	14.600	3.813	35.81	21.49	274.0	
B4N	14.450	3.807	35.34	21.49	305.9	
B5N	14.421	3.807	35.50	22.10	344.2	
B7N	14.397	3.818	32.95	20.00	233.2	
B9N	14.618	3.816	34.68	20.75	255.3	
B10N	14.557	3.817	33.86	20.33	191.7	
B6F	25.800	3.765	65.00	22.63	350.0	1000

[a]The properties of the fired core are measured after firing.

dx.doi.org/10.1021/ef402223d | Energy Fuels 2014, 28, 2092−2103

temperature; L and D are the length and diameter of the cores, respectively; PV and ϕ are the total effective pore volume and the porosity of the cores, respectively; K_b^0 is the initial absolute permeability of the core to brine. Unfired cores B2N to B10N are cut from the same batch; core B6F is fired at 1000 °C for a period of 6 h and belongs to a different batch. The temperature of the oven in firing is gradually increased in about 5 h to avoid thermal shock to the cores, as suggested by Wu and Firoozabadi.[25] We observe an increase in the core porosity and bulk density from firing.

The cores are initially washed with several pore volumes of methylene chloride, brine C, IPA, and methanol, and dried overnight in a convection oven at 150 °C prior to the flooding experiments. The unfired cores (B2N to B10N) are milled to 3.815 cm diameter for consistency and for better sealing between the core and the confining rubber sleeve. Saturation method is used to measure the effective porosity of the cores by following a protocol suggested by Worthington.[26] The cores are first covered by several layers of Kimwipes (to avoid core desaturation in the core handling), and they are placed in a saturation vessel. Vacuum of 6.7 Pa (50 mTorr) is applied to the saturation vessel for a period of 6 h; deaerated brine C (filtered to 60 μ) is then injected into the system using high pressure ISCO pumps and pressurized to 6.2 MPa for 16 h. After the porosity measurement, the fired core is covered by Teflon heat shrink tube before waterflooding tests to improve the mechanical strength.

2.2.2. Glass Micromodel. We investigate waterflooding of crude QO-2/brine K in a glass-etched micromodel. The length and width of the etched area of the micromodel are 6 and 4 cm, respectively, as shown in Figure 2a. The pore structure is shown in Figure 2b, and the pore structure properties are summarized in Table 4. Troughs are provided adjacent to the inlet and outlet pore spaces for uniform flow.

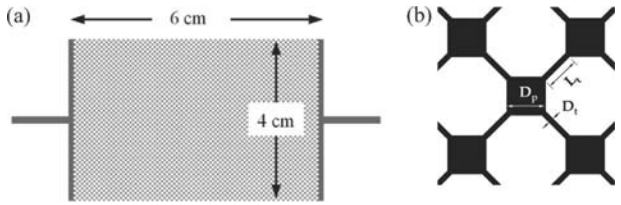

Figure 2. Glass micromodel (a) pattern dimensions and (b) pore structure.

Table 4. Pore Structure Characteristics of the Glass Micromodel

pore structure param.	value (μm)	range (μm)
pore size (D_p)	506.2 ± 4.1	474–542
throat size (D_t)	63.6 ± 2.3	2–91
throat length (L_t)	452.3 ± 4.2	428–480

2.3. Crude/Brine Emulsion Stability. Several crude samples from two different formations are used to investigate the formation of emulsions when mixed with either water or brines to screen them for the waterflooding tests. The stability and intensity of the crude/brine emulsions are qualitatively examined by mixing different crude samples with different brines at oil volumes of 25, 50, and 75%. After shaking the vials consistently for 1 min (using a rocking system), the samples are allowed to settle for a period of up to 15 months. Some of the crude samples are found to form tight emulsions. The term *tight emulsion* is used here for those stable emulsions for which the emulsion droplets are very fine, making it very difficult to demulsify.

2.4. Waterflooding Experiments. *2.4.1. Coreflooding Tests.* The core holder is placed horizontally in a convection oven with controlled temperature. The experimental set up is also maintained in a controlled environment to avoid temperature variation between the core holder assembly and the separation column. The core outflow in the waterflooding and permeability tests is drained to an atmospheric separator. The outlet pressure is atmospheric. The pressure of injecting brine and the temperature of oven, and controlled environment are recorded. A simplified schematic of process flow diagram for the waterflooding tests (in the cores) is shown in Figure 3.

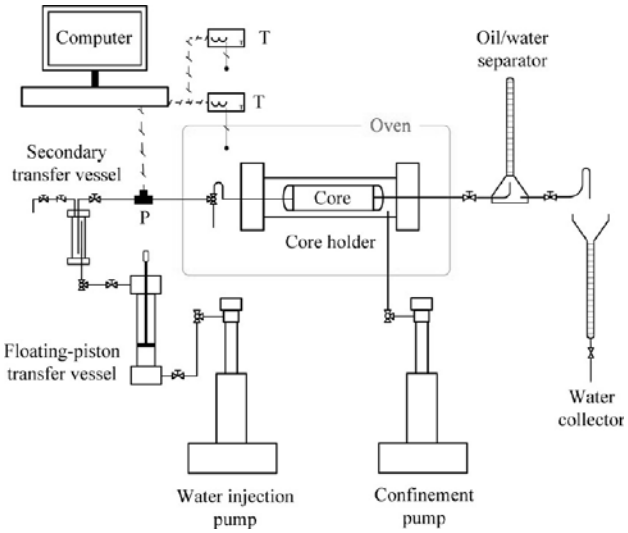

Figure 3. Simplified process flow diagram for the waterflooding tests in cores.

To saturate the core with liquids, a vacuum of 2.7 to 6.7 Pa is applied. After the core is evacuated to the desired vacuum for about 2 h, we close the outlet valve and inject about 2 PV of deaerated liquids, having a back pressure of 1379 kPa. The aging time for all experiments is provided in the last column of Table 5, which is 30 days for runs 1 to 4 and 20 days for runs 5 and 6. The waterflooding and aging processes are conducted at room temperature.

Table 5. Summary of Waterflooding Experiments

			injection rate			
run	oil ID	core ID	PV/d	cm^3/min	S_{wi} (PV)	aging time (days)
1	QO-2	B2N	5	0.120	0	30
2	QO-2	B3N	1	0.025	0	30
3	QO-9	B9N	5	0.120	0	30
4	QO-9	B7N	1	0.025	0	30
5	QO-2	B5N	5	0.123	0.269	20
6	QO-9	B4N	5	0.123	0.182	20
7	QO-13	B6F	4.4	0.200	0	3
8	QO-13	B6F	2.2	0.100	0	3
9	nC_7	B10N	5	0.118	0	3/4

For those runs with the initial water saturation, the core is initially saturated with the brine IW and displaced by the crude. As denoted in Table 1, the compositions of initial water and injection water (brine Q) are different. These compositions are based on the field data. To establish the initial water saturation, the core is placed vertically; the crude is injected from the top, producing water from the bottom. The outflow is sent to an oil/water separator, and the volume of produced brine IW is continuously monitored. After aging, we do not displace the oil in the core with fresh oil to avoid disturbing the initial water/oil emulsion in the core. The waterflooding experiments with the initial water saturation are conducted similar to those without the initial water saturation.

At the end of waterflooding experiments, the produced oil is transferred to 5 vials. We record the volume and weight of oil in each vial and then centrifuge it at 8000 rpm for a period of 1 h to examine the presence of emulsions in the produced oil.

Nine waterflooding experiments are conducted, as tabulated in Table 5. The first eight experiments are conducted with the crudes,

while the last experiment is conducted with nC_7 (as a reference). Our recent work[28] presents extensive flooding tests in the nC_7/brine system; the reader can refer there for more details. Injection rates of 1 and 5 PV/d are used in the waterflooding of the oils QO-2 and QO-9 in the unfired Berea cores. The rate effect is also examined in the fired Berea core B6F saturated with oil QO-13 and flooded at 4.4 and 2.2 PV/d. The effect of initial water saturation is investigated in the unfired Berea cores at the high injection rate in runs 5 and 6.

2.4.2. Visual Waterflooding. The waterflooding procedure in the micromodel are only slightly different than that in the cores; we initially vacuum the micromodel, then flood it with CO_2 followed by brine to establish the initial water saturation. A back pressure of 345 kPa is maintained, and CO_2 is dissolved in the brine and then displaced by several pore volumes of fresh brine. The micromodel is aged with brine or the crude (QO-2) for 18 h. These visual waterflooding tests are conducted at constant flow rates of 0.001 and 0.005 mL/min; the oilflooding (to establish the initial oil saturation) and waterflooding tests in the micromodel are observed at the pore-scale under a microscope. Pictures are occasionally captured from important pore-scale events such as emulsion formation, aggregation and coalescence, emulsion flow, pore blockage by emulsions, re-entrainment of emulsion to the flow stream, redistribution of water by snap off, direct invasion of water to displace oil, and the mobilization of trapped phase. The process is also video-recorded, occasionally.

2.4.3. Core/micromodel Cleaning. An extensive cleaning procedure is followed after a waterflooding experiment. The cleaning method is sensitive to the composition of crude.[27] We test the effectiveness of different solvents in glass test tubes and find that methylene chloride is more effective than toluene in dissolving crudes QO-2, QO-9, and QO-13; unlike toluene, methylene chloride does not alter the wettability. We clean a porous medium saturated with residual oil and brine by injecting 5 PV of methylene chloride, 3 PV of IPA, 2 PV of methylene chloride, 2 PV of IPA, and 1 PV of methanol. Nitrogen is then flooded into the porous medium for 1 h. Finally, we apply vacuum of 26.7 Pa for 1 h and dry overnight at 150 °C to remove the alcohols adsorbed on the solid surfaces. We also clean the micromodel with chromic acid 10% solution before saturating with brine and oil, and displace the acid solution with water, and dry it, as stated above.

3. RESULTS AND DISCUSSION

3.1. Emulsion Analysis. In a microscale perspective, the oil/water emulsion can be classified into simple emulsions of one phase into the continuum of another phase, such as o/w (oil-in-water) or w/o (water-in-oil) emulsions, and complex emulsions of both phases (multiple emulsions and bicontinuous). In a macro-scale view, the system of oil, water, and emulsion can be classified in terms of their phase behavior: type I (emulsion phase with excess oil), type II (emulsion phase with excess water/brine), type III (emulsion phase with excess of oil and water/brine), and type IV (emulsion phase with no excess of either oil or water/brine) as proposed by Winsor.[29] Emulsion phase behavior depends on temperature, salinity, pH, oil/water ratio, surfactant concentrations, applied shear, and molecular shapes.[30]

We observe the Winsor I, III, and IV behavior in the crude/brine mixture with oil volume fractions of 0.25, 0.50, and 0.75. Winsor IV was not stable and converted to either type I or III. A sample is taken from the emulsion layer and is viewed under microscope (KEYENCE VHX 2000), having red light exposure; the result is shown in Figure 4. This picture clearly shows the formation of w/o emulsions and also the aggregation and coalescence of water droplets. In this figure, the dark brown and creamy colors represent the oil and water, respectively. Interestingly, an interfacial film is detectable in most water droplets. Smaller water droplets are attached to a larger one while being separated from it through this interfacial film. In this work, we only observe the formation of w/o emulsions. Our observation is critically related to the challenges from waterflooding as we will discuss later.

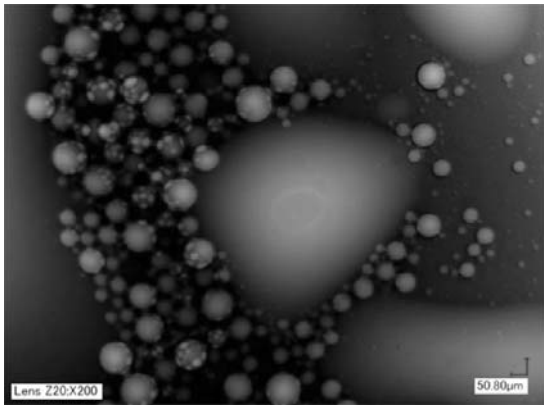

Figure 4. Microscopic view of aggregation and coalescence of water-in-oil emulsions. The picture is taken from the emulsion layer in Figure 1a.

We investigate the effect of brine, oil, and oil/water volume fractions on the emulsion stability in the glass vials. There are nine different crudes from different wells (CO, and QO-1, 2, 4, 7, 8, 9, 11, and 13). We mix these oils with nine different brines (brine 1−7, Q, and K), including the reservoir brine (Q) at three different oil volume fractions of 0.25, 0.50, and 0.75. We select the crudes QO-2, QO-9, and QO-13 for our flooding tests because they form tight emulsions with most brines. The strongest emulsion is formed by CO followed by QO-9. Figure 5

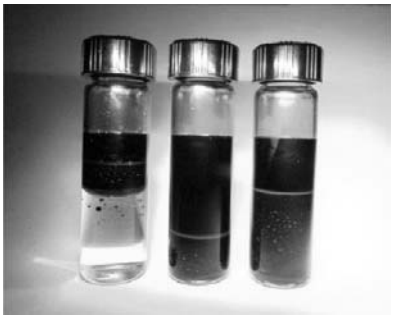

Figure 5. Stability of crude CO/brine 6 emulsion at time = 15 months for oil volume fractions of 0.25 (left), 0.50 (right), and 0.75 (middle). The vial contents are first mixed for 1 min.

shows a photo of 15-month long emulsion in the crude CO/brine 6 mixtures with the oil volume fractions of 0.25, 0.50, and 0.75. The vials shown in Figure 5 are consistently rocked for 1 min before settling. At the oil volume fraction of 0.25, Winsor III type is formed while at higher oil volume fractions of 0.50 and 0.75, only excess oil is observed, and Winsor type I is formed at equilibrium conditions.

Figure 6 compares the intensity of emulsions using five QO-series crudes with two brines Q and K. QO-9 is observed to form very tight emulsion with both brines—which are stable after 15 months. It follows that this crude forms a tighter emulsion with brine K, compared to brine Q; a thin layer of excess oil is observed for the QO-9/brine mixtures (Winsor-III type). The color change along the vials demonstrates the oil

segregation by gravity. QO-11 and 13 also form strong emulsions with both brines.

A fascinating observation in Figure 6a is the formation of emulsions at the crude/brine interfacial area (at the meniscus)

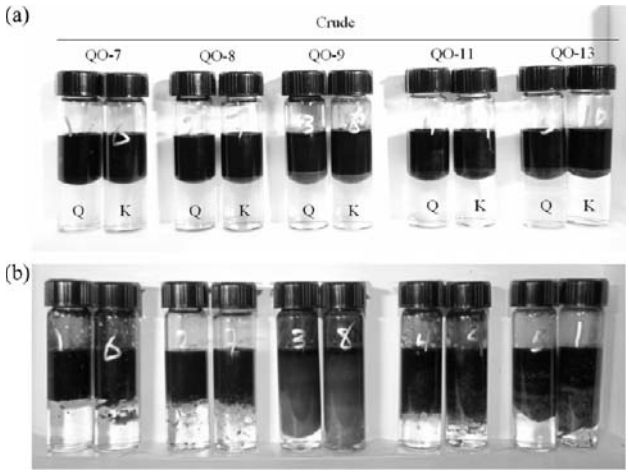

Figure 6. Emulsions in mixtures of five different crudes and two brines K and Q (oil volume fraction = 0.5): (a) 5 min after adding oil to water but before mixing and (b) 30 h after mixing. All vials are initially mixed for 1 min. The vials on the top and bottom match.

before mixing. In all vials, the oil is added to brines carefully to avoid mixing. Later we will confirm that the emulsion formation at the interface is of the w/o type, using tests in micromodel.

3.2. Waterflooding Experiments in Cores. *3.2.1. Production Performance.* Nine waterflooding experiments are conducted for which a summary of macroscopic production characteristics is provided in Table 6. The cores are saturated with emulsion-free crude oil (see Figure 1). Emulsions in the production stream or in the pores, if present, are formed in situ. Table 6 shows that the tests with the initial water saturation

Table 6. Waterflooding Results at Different Injection Rates by Invading Brine Q[a]

run	crude	Q_{inj} (PV/d)	S_{wi} (PV)	RF_{BKT} (HC PV)	RF_{Sor} (HC PV)	S_{or} (PV)
1	QO-2	5	0	0.235	0.602	0.398
2	QO-2	1	0	0.257	0.586	0.414
3	QO-9	5	0	0.150	0.554	0.446
4	QO-9	1	0	0.158	0.582	0.418
5	QO-2	5	0.269	0.357	0.422	0.424
6	QO-9	5	0.182	0.267	0.381	0.507
7	QO-13	4.4	0	0.260	0.588	0.412
8	QO-13	2.2	0	0.269	0.608	0.392
9	nC_7	5	0	0.492	0.493	0.507

[a]The brine initially in place is IW.

have lower final oil recovery, but surprisingly, higher oil recovery at the breakthrough. A comparison of runs 1 and 5 for the cores saturated with QO-2 show that the recovery at breakthrough is about 52% higher with the initial water saturation while the final recovery is about 30% lower in this case. A comparison of runs 3 and 6 demonstrates a 78% increase in the recovery at breakthrough for oil QO-9 with the initial water saturation, while the ultimate recovery is about 31% lower. For those runs with the initial water saturation, w/o emulsions are formed in situ during the oilflooding when we establish the initial oil saturation, and also during the aging time. The emulsion increases the apparent viscosity of the liquids in the core. Therefore, those runs with the initial water saturation suffer from adverse mobility ratio much more than the runs without the initial water saturation, yet they have higher recoveries at breakthrough. Note that if we had o/w instead of w/o emulsions, as observed in alkaline/surfactant flooding studies of heavy oils,[6−10,12,13] the formation of emulsion in brine is expected to improve the recovery at breakthrough, from the viewpoint of mobility ratio of displacing and displaced phases. Jennings et al.[31] explain the improved oil recovery at breakthrough (for the o/w emulsions) by decreased brine mobility—which eliminates water fingering or slows its growth.

Table 6 indicates that, without the initial water saturation, increasing the injection rate from 1 to 5 PV/d does not significantly affect the oil production performance of crudes QO-2, 9, and 13; the breakthrough time, final recovery, and residual oil saturations are not affected.

The cumulative oil production in terms of hydrocarbon pore volume (% HC PV) vs dimensionless time (HC PV injected) is plotted in Figure 7 for crudes QO-2 and QO-9, flooded with brine

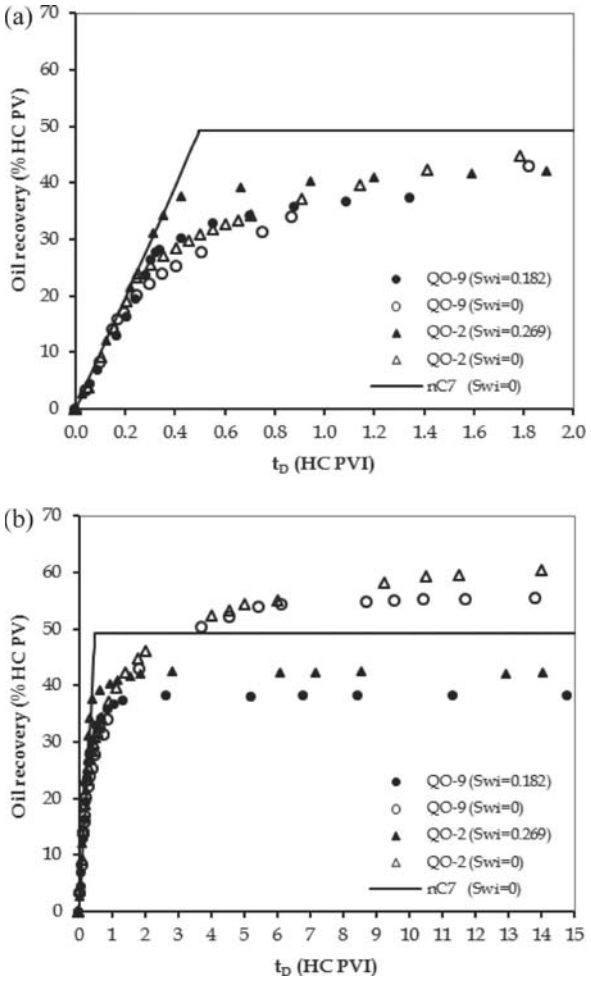

Figure 7. Oil recovery vs dimensionless time at 5 PV/d with and without initial water saturation for crudes QO-2, QO-9, and nC_7 oil at (a) 2 and (b) 15 PVI.

Q at an injection rate of 5 PV/d. The results are compared to waterflooding behavior of nC_7/brine Q (at the same rate) as a reference.

dx.doi.org/10.1021/ef402223d | *Energy Fuels* 2014, 28, 2092−2103

Figure 7a reveals that the initial water saturation can substantially delay the water breakthrough. This delay is induced by the emulsion droplet capturing and re-entrainments as discussed in the deep-bed filtration theory.[16−19] The pore blockage mechanisms by straining and interception are schematically shown in Figure 8. The core wettability also

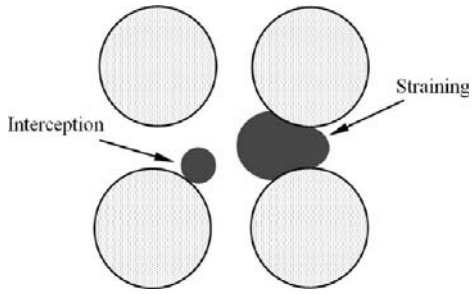

Figure 8. Pore space blockage by interception and straining mechanisms.

contributes to breakthrough in tests conducted at a similar mobility ratio. In those tests with higher connate water, the core is known to be less oil-wet; therefore, a higher recovery at breakthrough is expected from wettability. However, we point out that the experiments with the unusual crudes are remarkably more complex than the conventional immiscible displacement of Newtonian fluids; here, the interfacial rheology also substantially affects the flow behavior. We will see shortly in the visual test results that the crude/brine contact results in the formation of w/o microemulsions. These emulsions increase the viscosity of oil phase and make the displacing mobility ratio less favorable. In tests with higher connate water, more area is available to form emulsions and we expect higher w/o microemulsion concentrations (higher apparent oil viscosity) in the flowing stream. This means that the breakthrough should occur earlier from the analysis of mobility ratio. Yet, we observe a delayed breakthrough.

In establishing oil saturation in a core (saturated with brine and the subsequent establishment of irreducible water saturation), we refer to the oil injection stage as *oilflooding*. During the oilflooding, the pore-scale mixing of brine and oil occurs and the emulsions can form in the core. The emulsion droplet formation, aggregation, and coalescence may also occur during the aging. Consequently, a portion of the pore space will be occupied by the w/o emulsion droplets and connate water in the runs with the initial water saturation. With some pore spaces blocked, the flow of oil and water phases in the waterflooding will be rerouted to the channels with increased driving force; this makes the water flow pathway more tortuous, delaying breakthrough. The invading water phase can also collide with the captured emulsion droplets and be trapped temporarily, also delaying the breakthrough. These evidence are observed in waterflooding tests in the glass micromodel, to be presented shortly.

As shown in Table 6 and Figure 7a, the breakthrough occurs later in crude QO-2 (RF_{BKT} = 0.357 HC PV) with the initial water saturation of 0.269 PV, as compared to that for crude QO-9 (RF_{BKT} = 0.267 HC PV) with the initial water saturation of 0.182 PV. It is expected to see higher recovery at breakthrough for crude QO-2 because the displacing mobility ratio is more favorable (crude QO-9 is 4.3 times more viscous than QO-2). There is also additional benefit from wettability for the core saturated with QO-2 because it is expected to be more water-wet as a result of higher initial water saturation. Although the core saturated with QO-2 has significantly more connate water (48% more), the effect of connate water on breakthrough recovery enhancement (compared to no connate water) at 5 PV/d is more pronounced for QO-9 for which 78% increase in oil recovery at breakthrough is observed; this value is 52% for crude QO-2. For both cases, an additional absolute amount of about 12% HC PV recovery enhancement is obtained compared to the case with no initial water.

For all the crudes, the recovery at breakthrough is less than the recovery of the nC_7/brine system. This may be due to wettability condition of the core. The core saturated with nC_7 is expected to be more water-wet than that with the crudes. The crude can impose mixed wettability because of adsorption of heavier polar components onto the solid grains. Therefore, for the nC_7/brine system, the brine is directed to the continuum of smaller water-wet pore spaces along the core. The brine can accumulate at the outlet face without breaking through because of capillary discontinuity at the outlet face. Brine will build up in the core in the direction of reducing the capillary pressure. Close to residual oil saturation, the capillary pressure is substantially reduced and the brine can break through from the outlet face. At breakthrough, a recovery close to the final oil recovery is achieved; little oil is produced afterward.

As observed in Figure 7b, crude QO-2 has higher final recovery than QO-9; this observation is expected because the viscosity of QO-9 is about 4.3 times higher than that of QO-2; this makes the displacing mobility ratio less favorable for QO-9. At 5 PV/d injection, final oil recoveries of 60.2% and 55.4% are obtained for crudes QO-2 and 9, respectively, which are comparable despite the contrast in their viscosities.

Some pore bodies and pore throats can be blocked by w/o emulsions. This will result the oil flow being redirected to other channels, which causes delayed breakthrough. At breakthrough, some pore spaces that could have been invaded by brine (as they have minimum resistance to flow) are still blocked by the emulsion droplets. These regions may remain bypassed, if re-entrainment does not occur; permanent droplet capturing will result in lower final oil recovery. As seen in Figure 7b, little oil is produced after water breakthrough in tests with the initial water saturation, implying that most of the pore spaces with the captured emulsions are stay plugged.

In Figure 9, we show the effect of viscosity ratio of displacing to displaced fluids on the recovery performance of the liquid

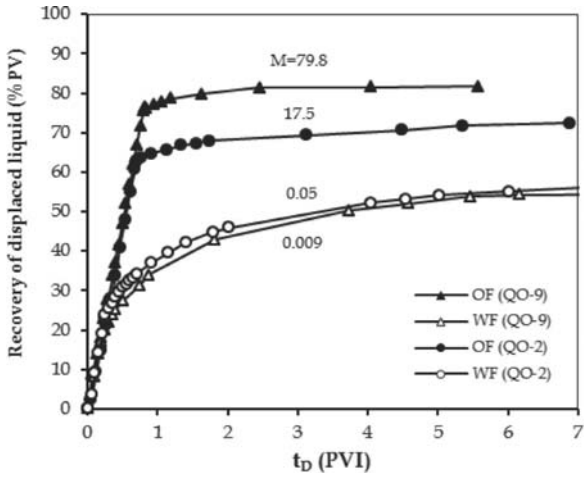

Figure 9. Oilflooding and waterflooding performances at 5 PV/d in cores saturated with liquid. *M* is the viscosity ratio of displacing-to-displaced fluids.

dx.doi.org/10.1021/ef402223d | *Energy Fuels* 2014, 28, 2092−2103

initially in place for crudes QO-2 and -9 and brines Q and IW. In this figure, recovery of displaced phase (brine in oilflooding, and crude oil in waterflooding, respectively) is shown versus dimensionless time. Note that the brines in the oilflooding and waterflooding are different. The brine used in the oilflooding is the initial water (brine IW) while the brine used in the waterflooding is the reservoir brine (brine Q). Figure 9 shows that the oilflooding results in higher liquid production (breakthrough and final recovery). Maximum recovery is for crude QO-9 (which is more viscous) displacing brine IW with a final water recovery of 81.8%; the final brine recovery with QO-2 is 73.1%. When water initially wets the grain surfaces in the oilflooding, the oil behaves like a nonwetting phase and therefore, invades into the continuum of larger pores. Because the oil is significantly more viscous than the water, the displacement process in the oilflooding is very efficient; most of the final water recovery is obtained at the time of breakthrough. Comparison of the waterflooding recoveries of crudes QO-2 and QO-9 up to about 7 pore volumes show little difference between these two crudes. Over longer times, crude QO-2 results in a higher oil recovery compared to QO-9 as observed in Figure 7b (after about 15 PVI).

At the end of the waterflooding experiments, the produced oil is centrifuged at 8000 rpm for 1 h. Except for Run 6, we do not observe emulsion production. Even for this run, we observe the production of only small amounts of emulsion. It is known that smaller droplets can diffuse deeper in porous media while larger droplets are captured in emulsion flow.[16−19] Crude oil QO-9 makes very fine emulsions (Figure 6b). Therefore, emulsions may percolate through porous media when compared to crudes QO-2 and -13, especially with the initial water saturation, and at higher injection rates. Although emulsion production has not been observed except in one run, we observe the production of w/o emulsions in the glass micromodels, because of the large sizes of the pore throats compared to a Berea core. The interpretation of pressure signal and production data also suggests the formation of w/o emulsions in the core. We will present these evidence shortly.

3.2.2. Pressure Response. Injection pressure data from waterflooding of the cores saturated with QO-2 and QO-9 at the high injection rate without the initial water saturation is shown in Figure 10. There are several features observed in this figure. First, there is an initial spike in the pressure. The pressure increases above the pressure drop required for the single phase flow of oil (at this rate) before the oil can flow. We will discuss this behavior shortly. Another characteristic of the pressure data in Figure 10 is the intense pressure fluctuations, for both crudes. The injection pressure in waterflooding from crude QO-9 is higher than that for QO-2; this behavior is expected because of the contrast in the viscosities of crudes QO-2 and 9. The viscosities of crudes QO-2 and QO-9 at room conditions (25 °C) are 19.3 and 82.2 cP, respectively. Using similar permeabilities and injection rate, higher injection pressure is expected in QO-9/brine. The experiment with QO-2 is conducted in core B2N with a permeability of 274mD as compared to the experiment with QO-9 conducted in core B9N with a permeability of 255 mD. Both cores have comparable diameter and length and only slight difference in the permeabily.

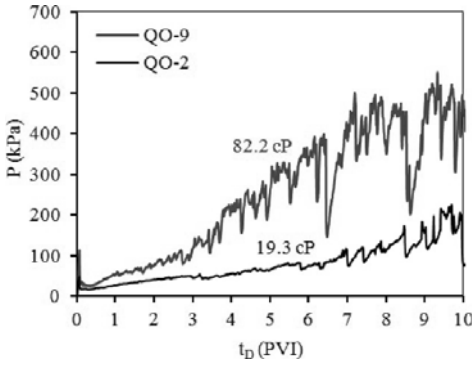

Figure 10. Effect of oil viscosity on injection pressure in waterflooding tests at 5 PV/d for QO-2 and QO-9 without the initial water saturation.

Large pressure fluctuations are believed to be due to a significant pore blockage (capture), and pore opening (re-entrainment), or perhaps by multiple captures and re-entrainments and because of the mobilization of the droplets. There can be either a pore throat blocked by a large water droplet via straining, or be partially blocked by the interception of a small droplet of emulsion (or multiple droplets). The pore blockage by interception of several emulsion droplets is observed in the visualization studies of waterflooding of a heavy oil.[32] Upon sudden pressure decrease and increase, the flow is significantly disturbed; this results in re-entrainment of captured droplets,[18] saturation redistribution upon secondary, tertiary, and etc. imbibition and drainage, and also the formation of emulsions because of created shear forces (pore-scale mixing). The sudden pressure decrease may be related to the trapped droplets squeezing through the pore constrictions. In that case, the pressure can build up to its original value before straining.[16−19]

Interestingly, the injection pressure is higher at the lower injection rate. This is shown in Figure 11a and b for crudes QO-2 and QO-9, respectively. At the lower injection rate, the pressure is higher and the pressure fluctuations are also more

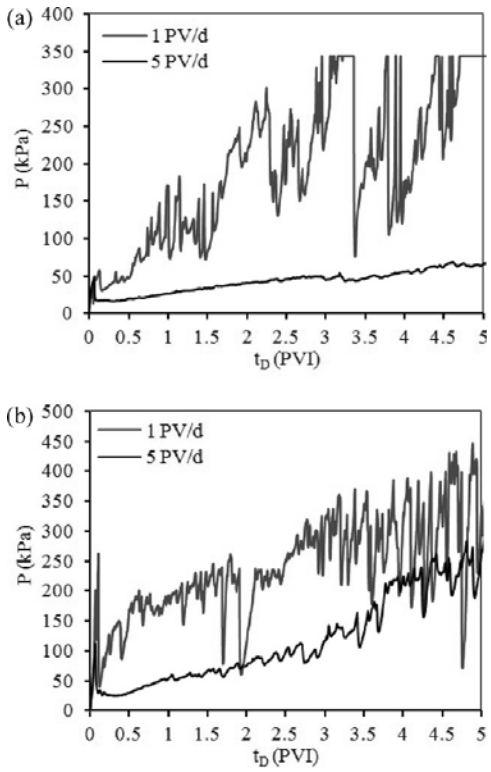

Figure 11. Effect of flow rate on injection pressure for (a) QO-2 and (b) QO-9 flooded at 1 and 5 PV/d.

intense. Similar observations are also made by Kumar et al.[8] who observed higher pressures in waterflooding of a heavy oil at a lower injection rate. Likewise, McAuliffe used o/w emulsions for the mobility control in the waterflooding and observed more local permeability reduction at lower injection pressures.[1]

All the mechanisms in the re-entrainment of the captured droplets (squeezing through constrictions, snap-off, and viscous break up) are velocity dependent and there are critical capillary numbers defined for these mechanisms in dilute and stable emulsion flow. The two mechanisms (squeezing and snap-off) are expected to have a similar critical capillary number ($\sim 10^{-4}$), while the critical capillary number for viscous break up is significantly higher (~ 1). Viscous break up is less probable to occur at capillary number conditions of waterflood.[18] Interception is governed by the interplay of hydrodynamic and electric double layer repulsion forces while re-entrainment is affected by the interplay of hydrodynamic and colloidal attraction forces. Both the processes are affected by the fluid velocity. Our data in Figure 11 show that re-entrainment is affected more by an increase in the injection rate from 1 to 5 PV/d as compared to capturing (i.e., less capturing and more re-entrainment occurs at high injection rates).

Furthermore, at low injection rates, because of longer contact time between the oil and brine phases the formation of emulsion may increase. For instance, in waterflooding of the QO-2-saturated core at 1 PV/d, we observe complete core blockage at about 12 PVI (as shown in Figure 12). In this

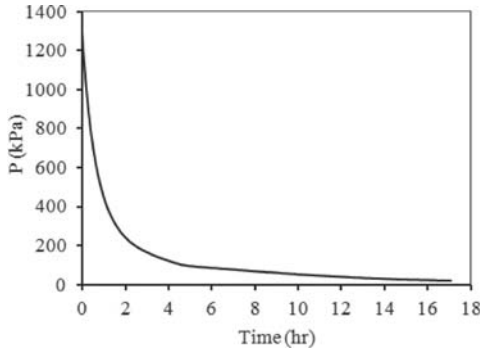

Figure 12. Depressurization at the end of waterflooding experiment (at 12 PVI) in QO-2 crude flooded at 1 PV/d.

experiment, we stop the injection after 12 PVI when the pressure increases to about 1288 kPa; it takes more than 18 h to depressurize the core. It seems that the core is blocked by the emulsion droplets. Note that, at the same pore volume injection, the core flooded at lower injection rate is exposed to brine 5 times longer. On the other hand, the intensity of oil/water mixing is higher in the core flooded at a higher rate. It seems that the prolonged contact time at lower injection rates affects emulsion formation more than the enhanced pore scale mixing at higher injection rates. Similar observation is also made in crude oil QO-13, which is flooded in fired core B6F; we do not present the result for brevity. We have conducted tests in fired cores to verify that the pressure fluctuations are not because of water adsorption onto clay surface.

Higher pressure drops at lower injection rates can be explained by pore-scale observations in the glass micromodel to be discussed in the next section. We find that at higher rates, multiple water/oil interfaces can advance in pore throats (adjacent to a pore body). Therefore, the concentration of w/o emulsions at the flowing stream in pore throats is less, resulting in lower apparent viscosity.

There is another interesting feature in the injection pressure data. At steady-state, a fixed pressure drop allows the single phase oil to flow in the core at a specific rate. However, when the waterflooding experiment is started (at the same rate), the injection pressure increases significantly above the steady-state pressure drop of single phase oil before the oil can flow in the core. The injection pressure data at the injection rate of 5 PV/d are presented in Figure 13; the pressure spikes are higher in

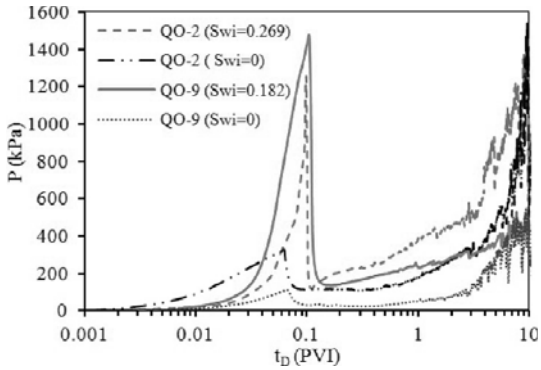

Figure 13. Injection pressure in waterflooding tests with and without the initial water saturation, at 5 PV/d.

tests with the initial water saturation. For example, for waterflooding of oil QO-9 with the initial water saturation of 18.2% PV, the pressure raises to about 1551 kPa before the oil continuum flows. Note that the pressure later drops to about 172 kPa. At this pressure, the liquid could readily flow in the core; however, a higher pressure is required for flow initiation. This spike is less in tests without the initial water saturation. For example, for the same crude to flow at the same injection rate with no initial water saturation, a peak pressure drop of 112 kPa is observed while at 30 kPa, the liquids can flow in the core; w/o emulsions increase the viscosity of continuous phase; the viscosity of emulsion is found to exponentially increase with volume fraction of the dispersed phase up to the emulsion inversion point.[33]

Pressure spikes can be due to inertia, high mobility ratio, oil shear thinning behavior and also the oil/water viscoelasticity. The core permeability and injection rate also govern the intensity of the spikes. The oil exhibits only a mild shear thinning characteristic as seen in Figure 14. We do not observe a pressure spike in the permeability measurement to oil where fresh oil displaces the aged oil in the core. The injection pressure increases from zero and approaches the pressure drop of the single phase oil.

The final pressures at 10 PVI (at the same injection rate) are comparable for crude QO-9 with and without the initial water saturation. The implication is that with no initial water, the emulsions form in situ as well. By comparing the pressure behavior of crudes QO-2 and QO-9, it follows that despite the contrast in oil viscosities, a higher pressure drop is attained for the lighter oil (except for the early time). The initial pressure spikes are comparable for these two crudes.

3.3. Waterflooding Experiments in Glass Micromodel.

We saturate the micromodel with brine and flood it by oil at 0.001 and 0.005 mL/min. It is observed that the oil can rupture

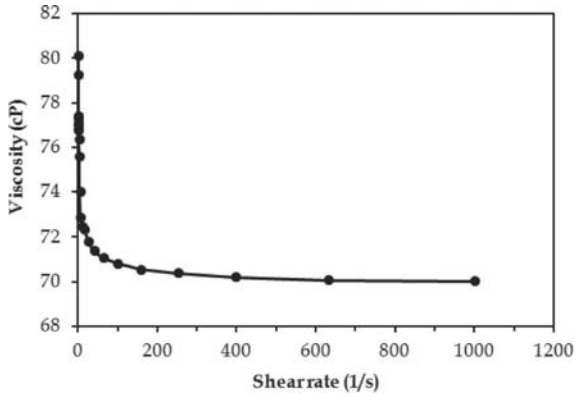

Figure 14. Viscosity of QO-9 vs shear rates.

the film of water on the pore surfaces. Water only remains in the pore throat and also in the pore spaces connected with fine pore throats. We eventually observe the fractional wettability condition in which the continuum of large pore spaces is wetted by the oil phase. The sequence of oil/water interface advancement in the oilflooding is shown in Figure 15 for a fixed pore space frame. This figure shows how the water and oil distribute initially in the pore spaces (before waterflooding). In the pore-scale photos, S, W, O, and A represent the solid, water, oil, and air, respectively. In Figure 15a, the oil invades a pore body saturated with brine. The pore body is fully invaded by the oil in the sequence shown in Figure 15b–e. The oil ruptures the film of brine on the pore surface and occupies the pore. In Figure 15f, the oil invades two pore throats attached to the pore body. Brine becomes trapped in one of the pore throats, (with the lowest breakthrough capillary pressure). After the core is aged for 18 h, it appears that the pore surface stays water-wet in the pore throats where the oil has not initially displaced the water; the continuum of large pores, however, becomes oil-wet.

Now, we focus on examining the emulsion formation (see Figure 16). We observe both w/o microemulsions and w/o macroemulsions, which are captured during the oilflooding. The macroemulsions mostly form by the snap off of the water phase, and to a lesser extent, by the aggregation and coalescence of microemulsions. The microemulsions form at the interface of oil and water in both the oilflooding and waterflooding. The microemulsions are stable and are carried by the flowing stream.

To ensure that the droplets seen in Figure 16 are not solid particles, we conduct an oilflooding test in which the micromodel is initially saturated with air and then flooded

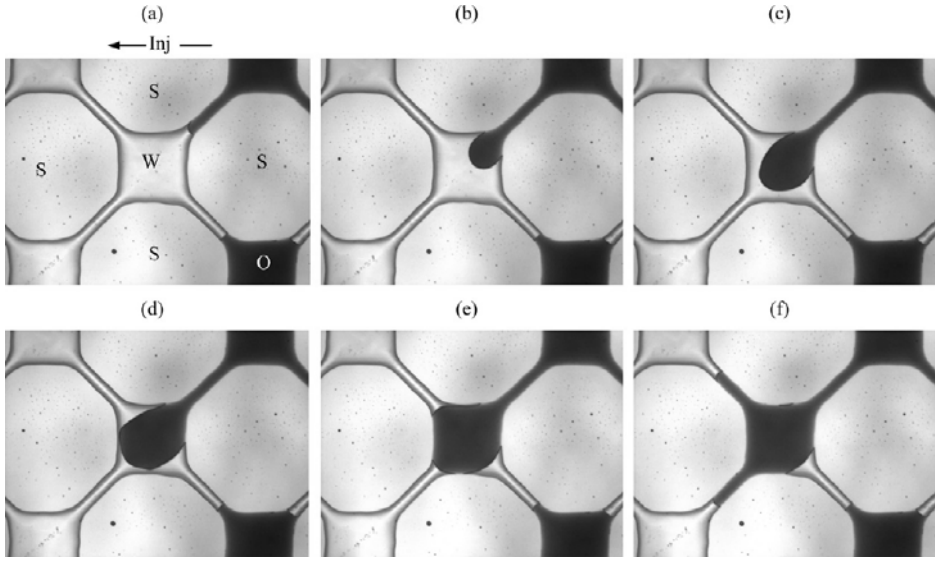

Figure 15. Sequence of oil/water interface advancement in oilflooding QO-2 in micromodel saturated with brine K at 0.001 mL/min. The dark color represents the oil phase and the light color represents water phase. The letters a–f show the sequence of invasion.

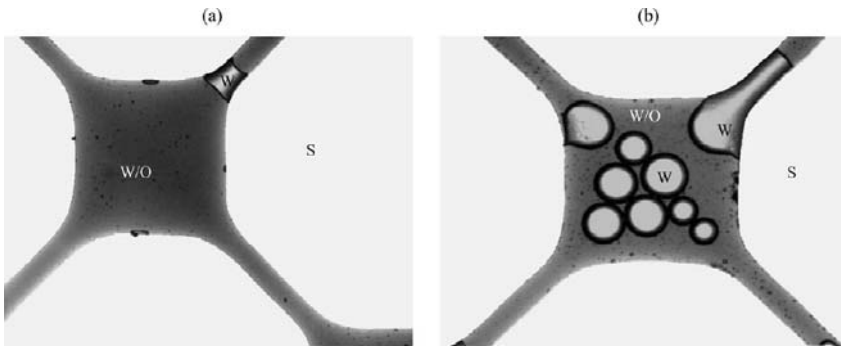

Figure 16. Formation of (a) microemulsions and (b) micro- and macroemulsions in oilflooding in QO-2/brine K system at 0.001 mL/min. The black spots are w/o microemulsions.

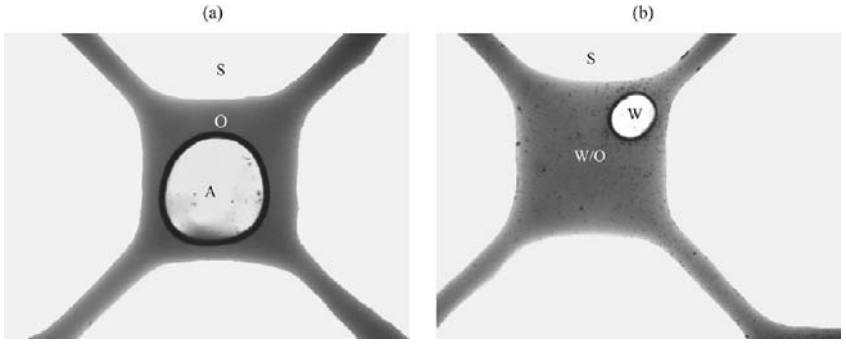

Figure 17. Oilflooding of air-saturated and brine-saturated; (a) QO-2/air and (b) QO-2/brine system at 0.001 mL/min.

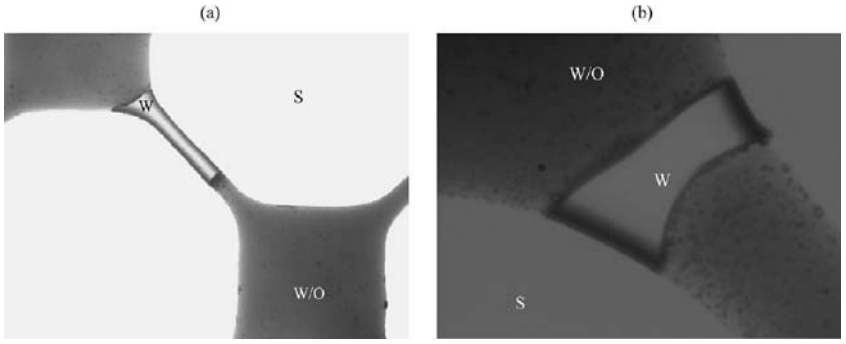

Figure 18. A ccumulation of w/o emulsion at the water/oil interface in the QO-2/brine K system during oilflooding: (a) low magnification, 0.001 mL/min and (b) high magnification, 0.005 mL/min.

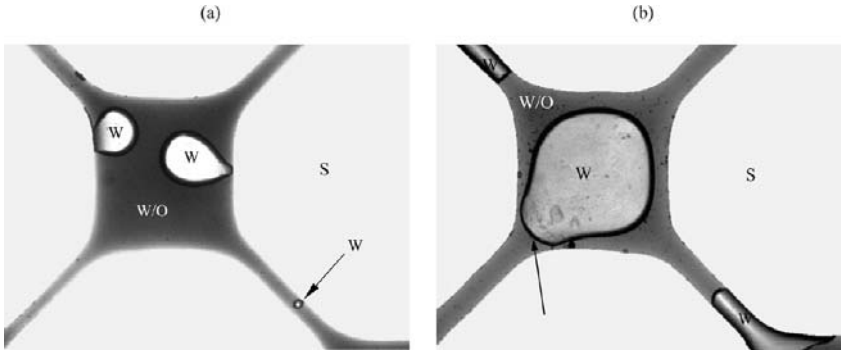

Figure 19. Pore blocking by water droplets via (a) interception and (b) straining for the QO-2/brine K system, rate 0.001 mL/min.

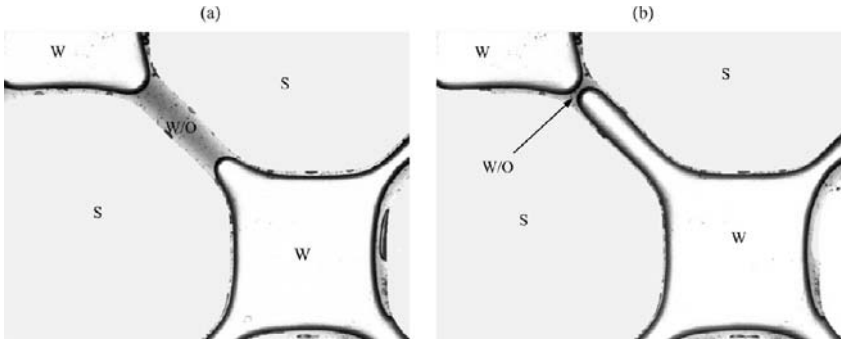

Figure 20. Effect of rate on mobilization of emulsions at (a) 0.001 (ΔP = 12.4 kPa) and (b) 0.005 mL/min (ΔP = 28.3 kPa) for QO-2/brine K system.

with the oil. The result is shown in Figure 17a for a pore filled with trapped air and oil. It is clear from this figure that there are no black spots in the oil phase, whereas in Figure 17b we observe a large number of black spots, which represent w/o emulsions. Similar observations are made for other pore spaces of the micromodel.

dx.doi.org/10.1021/ef402223d | *Energy Fuels* 2014, 28, 2092−2103

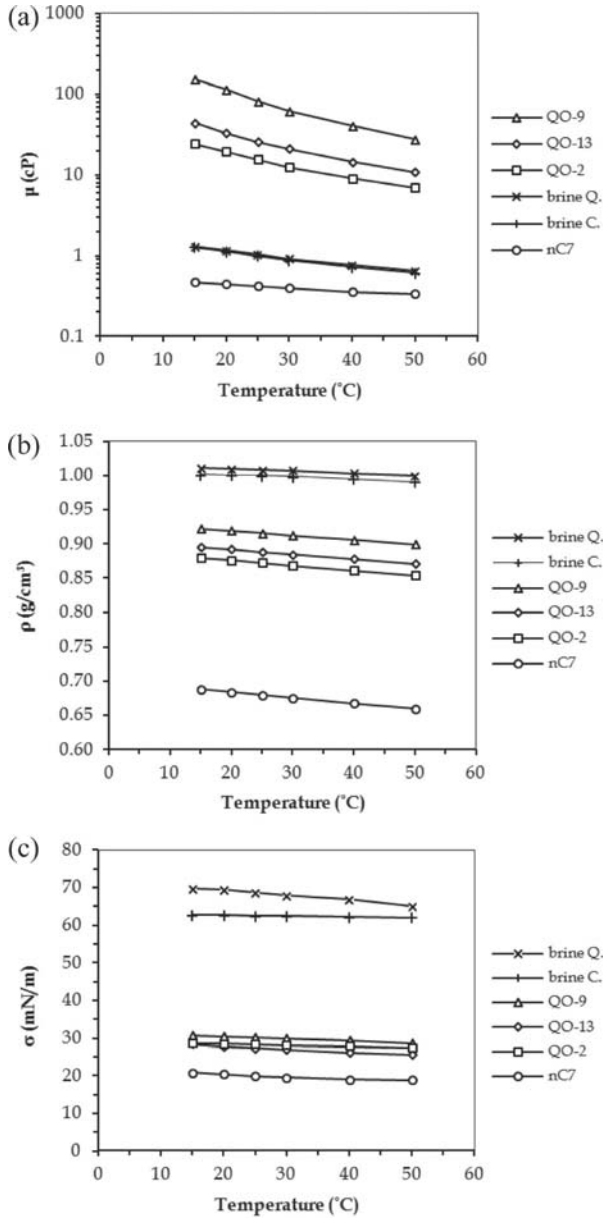

Figure 21. Temperature dependency of the physical properties of fluids used in the range 15−50 °C: (a) viscosity, (b) density, and (c) surface tension.

The microemulsion droplets flow with the oil phase. They accumulate at the oil/water interface and at dead-end pore spaces. The accumulation of w/o microemulsions at the oil/water interface is shown in Figure 18a at the right interface. The high apparent viscosity of the interface region from high concentration of w/o emulsion slows flow. Figure 18b shows a highly magnified picture of another pore throat with a high density of water droplets. At high injection rates, re-entrainment of microemulsion droplets to the main flow stream is observed and the emulsion droplets become more dispersed.

In the waterflooding tests in the micromodel, we observe pore blockage by straining and interception of w/o emulsion droplets. We show the pore-scale view of pore blockage for the interception and straining in Figure 19. A pore is observed to be blocked by droplets larger or smaller than the pore throat, as shown in Figure 19a. We find that when a water droplet blocks a pore, it disturbs the flow stream, redirecting the emulsion flow from that pore space.

The effect of injection rate on pore-scale behavior of waterflooding is shown in Figure 20. We increase the flow rate from 0.001 to 0.005 mL/min and focus on the pore-space shown in Figure 20. The additional driving force helps to squeeze the water phase through its adjacent pore constriction, resulting in recovery of oil in the pore throat. The injection pressures in Figure 20 are 12.4 (at 0.001 mL/min) and 28.3 kPa (at 0.005 mL/min). At later time, the advancing water/oil interface shown in Figure 20b pushes out the oil in the pore throat, and the two water phases collapse.

In general, the following observations are made when increasing the flow rate:

- More oil is displaced by invasion of multiple water/oil interfaces into the pore bodies and pore throats.
- More snap-off occurs, resulting in redistribution of the water phase and the formation of macroemulsions.
- Re-entrainment of captured droplets of w/o emulsions to the main flow stream occurs.
- The trapped phase is more likely to be mobilized.
- The w/o emulsions become more dispersed. At high injection rates, multiple oil/water interfaces can advance in the pore throats adjacent to a pore body. Thus, the local concentration of emulsions in the flow stream can be diluted by the dispersion of droplets.

4. CONCLUSIONS

Based on extensive experimental results of the unusual crudes, which form tight emulsions, we draw the following conclusions:

- w/o microand macroemulsions may form in situ by waterflooding, even without the initial water saturation.
- The waterflooding results show negligible effect of injection rate on oil production history (in the range of employed capillary numbers) when no initial water saturation is present.
- Significant pressure fluctuations may occur in the waterflooding process when w/o emulsions are formed. The fluctuations can be explained by the emulsion droplet capture and re-entrainment.
- The magnitude of pressure and pressure fluctuations are larger at lower injection rates.
- A pronounced pressure spike may be observed at early time, especially with the initial water saturation.
- Initial water saturation significantly hinders the breakthrough time. However, the final oil recovery is significantly lower with the initial water saturation.
- Despite the evidence for the formation of w/o emulsions in the porous media, we may not observe the percolation of emulsion droplets in the produced stream.
- Tight w/o emulsion is observed at the interface between the oil and water. The interface viscoelastic behavior may be an important topic in future studies.
- The production behavior of crudes, which form w/o emulsions at the lab scale, suggests severe production challenges by the conventional waterflooding due to high pressure drops.

■ APPENDIX

The temperature-dependency of physical properties of the crudes and brines are shown in Figure 21 in the temperature

range 15−50 °C. The viscosities of fluids are measured by capillary viscometers (Cannon-Fenske, No. 25, 100, and 200); the densities are measured by pycnometers (10 mL Gay−Lussac, Wilmad-LabGlass), and the surface tension values are measured by plate tensiometer (K12 Processor Tensiometer, Krüss).

■ AUTHOR INFORMATION

Corresponding Author

*E-mail: abbas.firoozabadi@yale.edu.

Notes

The authors declare no competing financial interest.

■ ACKNOWLEDGMENTS

The support by the members of the consortium of Reservoir Engineering Research Institute (RERI) ,and by Maersk R&D Qatar, is greatly acknowledged. Various discussions and suggestions by Dr. Kristian Mogensenof Maersk R&D Qatar were very helpful to the research project, and we thank him for his interest throughout the work. We also thank Prof. Clayton J. Radke of the University of California Berkley for the valuable discussions. The authors also acknowledge Prof. Gerald G. Fuller and Mr. H.-K Dong of Stanford University for the bulk and interfacial rheology measurements. We thank Qatar Petroleum for the permission to publish the work.

■ REFERENCES

(1) McAuliffe, C. *J. Pet. Technol.* **1973**, *6*, 727−733.
(2) McAuliffe, C. *J. Pet. Technol.* **1973**, *6*, 721−726.
(3) DeZabala, E.; Radke, C. *SPE Reservoir Eng.* **1986**, *1*, 29−43.
(4) Kokal, S. *SPE Prod. Facil.* **2005**, *1*, 5−13.
(5) Tambe, D. E.; Sharma, M. M. *J. Colloid Interface Sci.* **1994**, 1−10.
(6) Bryan, J.; Mai, A.; Kantzas, A. *SPE/DOE Symposium on Improved Oil Recovery*, 2008.
(7) Bryan, J.; Kantzas, A. *J. Can. Pet. Technol.* **2009**, *2*, 37−46.
(8) Kumar, R.; Dao, E.; Mohanty, K. *SPE J.* **2012**, *2*, 326−334.
(9) Liu, Q.; Dong, M.; Yue, X.; Hou, J. *Colloids Surf. Physicochem. Eng. Aspects* **2006**, *1*, 219−228.
(10) Liu, Q.; Dong, M.; Ma, S. *SPE/DOE Symposium on Improved Oil Recovery*, 2006.
(11) Dong, M.; Ma, S.; Liu, Q. *Fuel* **2009**, *6*, 1049−1056.
(12) Dranchuk, P.; Scott, J.; Flock, D. *J. Can. Pet. Technol.* **1974**, *3*.
(13) Farouq Ali, S.; Figueroa, J.; Azuaje, E.; Farquharson, R. *J. Can. Pet. Technol.* **1979**, *1*.
(14) Green, D. W.; Willhite, G. P. *Enhanced Oil Recovery*; Society of Petroleum Engineers: Richardson, TX, 1998.
(15) Alvarado, D. *SPE J.* **1979**, *6*, 369−377.
(16) Soo, H.; Radke, C. *Chem. Eng. Sci.* **1986**, *2*, 263−272.
(17) Soo, H.; Radke, C. J. *Ind. Eng. Chem. Fundam.* **1984**, *3*, 342−347.
(18) Soo, H.; Radke, C. *J. Colloid Interface Sci.* **1984**, *2*, 462−476.
(19) Schmidt, D. P.; Soo, H.; Radke, C. *SPE J.* **1984**, *3*, 351−360.
(20) Dake, L. P. *Fundamentals of Reservoir Engineering*; Elsevier Science: Amsterdam, 1978.
(21) Lake, L. W. *Enhanced Oil Recovery*; Prentice Hall, Inc.: Englewood Cliffs, NJ, 1989.
(22) Donaldson, E. C.; Chilingarian, G. V. *Enhanced Oil Recovery: Processes and Operations*; Elsevier Science: Amsterdam, 1985; Vol. *2*.
(23) Slider, H. C. *Worldwide Practical Petroleum Reservoir Engineering Methods*; PennWell Corporation: Tulsa, OK, 1983.
(24) Sheng, J. *Modern Chemical Enhanced Oil Recovery: Theory and Practice*; Gulf Professional Publishing: Houston, TX, 2010.
(25) Wu, S.; Firoozabadi, A. *Energy Fuels* **2011**, *25*, 197.
(26) Worthington, A. *J. Pet. Technol.* **1978**, *12*, 1716−1717.
(27) Gant, P.; Anderson, W. *SPE Form. Eval.* **1988**, *1*, 131−138.
(28) Rezaei, N.; Firoozabadi, A. *SPE J.* **2014**, submitted.
(29) Winsor, P. *Trans. Faraday Soc.* **1948**, 376−398.
(30) Ghosh, P. *Colloid and Interface Science*; Phi Learning: New Dehli, 2009.
(31) Jennings, H. Y.; Johnson, C. E.; McAuliffe, C. D. *J. Pet. Technol.* **1974**, *12*, 1344−1352.
(32) Mei, S.; Bryan, J.; Kantzas, A. *SPE Heavy Oil Conference Canada*; 2012 .
(33) Richardson, E. *J. Colloid Sci.* **1950**, *4*, 404−413.